Aerodynamic Performance Characterization and Structural Analysis of Slotted Propeller: Part A Effect of Position

Aravind SEENI*

*Corresponding author
School of Aerospace Engineering, University of Science Malaysia,
Engineering Campus, Nibong Tebal, Penang 14300, Malaysia,
aravindseeni@gmail.com

DOI: 10.13111/2066-8201.2020.12.2.16

Received: 30 October 2019/ Accepted: 02 February 2020/ Published: June 2020

Abstract: *Novel slotted propeller design performance is presented in terms of thrust coefficient, power coefficient and efficiency by utilizing ANSYS Fluent. The effects of slotted positions were discussed with respect to baseline APC Slow Flyer 10' x 7' configurations. Seven slot locations with respect to chord length(c) namely 12.5%c, 25%c, 37.5%c, 50%c, 62.5%c, 75%c and 87.5%c were tested. The result shows that introduction of slot along the propeller blade increases the thrust coefficient, in the range of 0.1% to 4.74% for low advance ratios. However, increase in thrust coefficient also increases power coefficient compared to baseline design, hence reducing propeller efficiency. In addition, structural integrity of the blade was tested. The pressure distribution of the propeller blade demonstrated higher pressure on the back section, and lower pressure at the front section which results in thrust. In addition, the result shows that the pressure distribution is highly influenced by changes in advance ratio. The analysis shows that the novel propeller design managed to withstand stress and strain breaking point when operated at high advance ratio.*

Key Words: *slotted propeller, computational fluid dynamics, static structural, low Reynolds number, APC Slow Flyer, ANSYS Fluent, ANSYS Mechanical*

1. INTRODUCTION

Continuous development and optimization of Unmanned Aerial Vehicle (UAV) design throughout the past years are mainly due to the rapid growth in design and development of system and components required. The availability of advanced lightweight material, microelectronics system, allowing design of enhanced efficiency UAV has made this possible. The growth has resulted in emergence of civil market and its utilization of UAV for various missions [1]–[3].

The efficiency of a UAV is significantly influenced by the propeller. Thus, the propeller selected for any UAV need to be able to cater to the aerodynamic design requirements of the UAV. Currently, the selection of propeller blade is performed from off-the-shelf based on its availability and economical advantage. Therefore, more efforts are required to find suitable propeller blade based on the UAV design.

In addition, the implementation of unconventional blade design such as slotted, serrated, tubercle and adaptive structure are barely used in any UAV. This is due to lack of research in unconventional design specifically for low Reynolds number small-scale propeller. Therefore,

this study aims to provide an extensive research on novel slotted designs for small scale propeller blade operating at low Reynolds number, typically at 68500 measured at 75% blade station location along span.

The objective of this work is to design and study the performance of slotted propeller blade operating at low Reynolds number. The study is divided into two main analyses, namely aerodynamic performance and static structural analysis. The flow simulations are performed through three-dimensional computational fluid dynamics software ANSYS Fluent to determine the thrust coefficient, power coefficient and efficiency measured in different flow conditions. Meanwhile ANSYS Mechanical Static Structural is used to determine the highest stress and maximum deformation experienced by the propeller blade. The next section discusses the methodology and design available for UAV, marine ship and wind turbine, as these blades working principle is similar, varying only in shape for working conditions adaptations [4], [5].

Extensive research has been done for the conventional design of propeller, revolving around the standard parameters of diameter, pitch, blade shape and chord length. Thus, the opportunity available to further improve the design of propeller is by inducing more advanced design, such as serrated, slotted, tubercled and/or adaptive structures. Liu et. al [6] performed a study to investigate the impact of serration on leading and trailing edge of airfoil. The result shows conditional performance due to major influence of serration design and airfoil type. Apart from that, Chong [7] discussed various serration design, including M-shaped, wavy and saw-tooth. Based on the analysis, it is proven that serration influences boundary layer characteristics.

Ibrahim et al. [8] tested two advance blade design, including slotted and tubercle for wind turbine. The result shows that slotted design performed better than straight blade in terms of power, while tubercled design's performance decreases. Lin et al. [9] compares the performance of tubercled blade wind turbine with straight design. The result shows an improvement of 0.38% to 2.31% increase in thrust. In addition, Belamadi et al. [10] studies the performance of slotted wind turbine airfoils. Both leading edge and trailing edge designs were tested, which gives the result that implementation of slotted design does not always lead to performance improvements, as it depends on the position and size of the slots.

There are two main methods available to determine the performance of a propeller, namely the experimental and the numerical method. Apart from experimental analysis, the numerical analyses is now commonly selected for performance analyses among researchers. This is due to its capability to determine wide variety of results, such as forces and pressure. In most research, integration of both methods are used to validate numerical method results by comparing them with corresponding experimental outcomes.

In experimental method, the propeller blade is tested in the wind tunnel. Brandt et al. [14] performed an experimental study to determine the performance of 79 small scale low Reynolds number propeller with variation of rotational speed. In addition, Deters et. al [15] performed a similar experimental study for 27 different types of propeller to study the influence of Reynolds number on propeller blade performance.

Subhas et al. [16] performed a numerical study to study the performance of ship propeller by using CFD method, utilizing Multiple Reference Frame (MRF) approach. The results obtained were compared with experimental analysis, with maximum and minimum difference of 0.0013 and 0.001, respectively. Wang et al. [17] performed a study to determine the performance of the propeller blade by using CFD incorporating transitional analysis. In addition, Benini [18] utilized CFD Fluent to determine the performance of marine propeller. The result shows a slight discrepancy in experimental data at a maximum of 5%. Tian et al.

[19] studied the performance of wind turbine using Fluent, utilizing sliding mesh method to incorporate the blade rotation. The result shows that the error between experimental and numerical data is below 5%, which proves that numerical method is acceptable for performance prediction.

Apart from propeller performance, reliability of a propeller blade also depends on its structural integrity. Seetharama et al. [20] performed a stress analysis on composite propeller by using finite element analysis (FEA) using ANSYS. The study discussed and proposed the methodology for designing and analyzing the composite and metal propeller blade, in terms of maximum deformation and normal stress.

Yeo et al. [21] predicted blade stress distribution for marine propeller blade through FEA. The analysis utilized the pressure distribution along the blade, to determine the highest stress and maximum blade deflection. Additionally, Das et al. [22] did a study to compare the blade performance of the blade before and after deformation. The study found that the performance is not affected as the blade is rigid enough causing very minimal blade deformation.

Kishore et al. [23] compared structural performance of two different materials for propeller blade, by analysis through ANSYS. Von-Mises maximum stress and strain, and total deformation data were collected. The results obtained from the analyses were compared with the material mechanical properties.

2. METHODOLOGY

In this study, off-the-shelf APC Slow Flyer 10'x7' propeller blade is set as standard baseline design, due to the availability of experimental data. Details on APC Slow Flyer are further explained in the next section. As mentioned previously, this study focuses on two main analyses, which are the aerodynamic performance and the static structural analysis. First, the numerical simulation of baseline design APC Slow Flyer is performed using commercially available ANSYS Fluent software. This is intended to validate the numerical method to extract the propeller performance characteristics.

The results obtained from the numerical analysis are compared with experimental data available in [15], [24]. Then, by using the validated method, similar analyses are done for newly developed slotted propeller blade design. The results are then compared with the baseline APC Slow Flyer to determine the performance improvements of novel slotted blade design. To determine the structural integrity, the best performance slotted design undergo further analyses by utilizing ANSYS Static Structural, to estimate the maximum stress, maximum strain and total deformation under pressure.

2.1 Propeller model

The APC Slow Flyer is a small scale two-bladed propeller, with a diameter of 0.254m. The propeller consists of Eppler E63 sections near the hub and Clark-Y sections near the tip. Fig. 1 shows the three-dimensional model of the blade, created using CATIA V5.

Fig. 1 - APC Slow-Flyer 10'x7' baseline design

2.2 Computational Fluid Dynamics (CFD)

2.2.1 Computational Parameters

The computational domain is divided into stationary region and rotating region. The stationary domain is a cubic design and the distance used for the stationary region is 4D upstream and 4D downstream to prevent the recirculation of flow in the rotating region that will influence the result of the analysis. The domain is defined and illustrated in Fig. 2(a). Meanwhile the rotating region is set to be 0.4D thickness with 1.1D diameter of enclosure. The propeller blade is embedded in the cylindrical rotating domain as shown in Fig. 2(b). The rotation of this domain was achieved with Multiple Reference Frame [11], [12], [13].

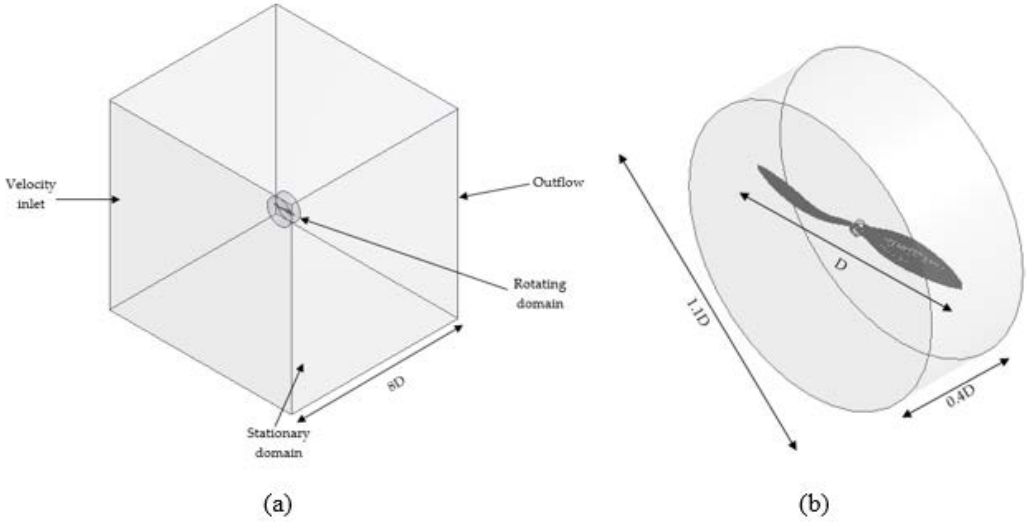

Fig. 2 - Flow domain and boundary conditions. (a) Stationary domain with rotating domain in enclosure (b) Rotating domain

2.2.2 Mesh Generations

The grid is composed of fully tetrahedral, unstructured mesh for the entire domain. The selection of fully tetrahedral mesh is based on the justification that the grids have the capabilities to discretize complex geometries with minimum user intervention. In addition, it requires less computational time and manages to capture the boundary layer condition to ensure satisfactory analysis. To capture the boundary layer better, the mesh is made to be more refined along the blade. This is to ensure more meshing is concentrated along the blade region, as it influences the accuracy of the analysis, rate of convergence and computational time required.

2.2.3 Boundary conditions

The analyses were conducted for range of advance ratios from 0.192 to 0.799 and corresponding free-stream velocities at inlet. A fixed rotational speed of 3008 rpm is assumed. On the inlet flow domain, the inlet velocity is set as tabulated in Table 1.The turbulence intensity is set to be 0.1%, based on the experimental analysis by [14], [15], [24].
At the outlet boundary condition, it is set as outflow. Outflow is selected for the condition in which there is no information on the exit flow such as velocity or pressure prior to the analysis. In addition, the rotation of the rotating domain was achieved with Multiple Reference Frame by incorporating rotational speed of the propeller.

In addition, the pressure-coupling is achieved by using SIMPLE (Semi Implicit Method for Pressure Linked Equations) algorithm. Second order upwind is applied for momentum interpolation. First order upwind scheme is selected for turbulent kinetic energy and specific dissipation rate.

Table 1. - Simulation flow conditions

Advance coefficient, J	Free stream velocity (m/s)
0.192	2.4384
0.236	2.9972
0.282	3.5814
0.334	4.2418
0.383	4.8641
0.432	5.4864
0.486	6.1722
0.527	6.6929
0.573	7.2771
0.628	7.9756
0.659	8.3693
0.717	9.1059
0.773	9.8171
0.799	10.1473

2.3 Static Structural Analysis

In this computational analysis, the structural analysis of the propeller blade was investigated by utilizing ANSYS Static Structural. The sections below describe the setup required to determine von-Mises maximum stress, von-Mises maximum strain and total deformation.

2.3.1 Engineering Data

For this analysis, the material used are long fiber thermoplastic, specifically 60% long strand glass fiber reinforced nylon 6 Natural, similar to realistic APC Slow Flyer 10’x7’ propeller blade. The mechanical properties data are collected from the manufacturer site [25]. The details of the material properties are listed in Table 2.

Table 2. - Material properties

Property	Value
Density	1690 kg/m^3
Young's Modulus	19500 MPa
Poisson's Ratio	0.44
Stress at break	250 MPa
Strain at break	1.58%

2.3.2 Meshing

Once the slotted propeller model is transferred into ANSYS Workbench, the mesh is generated with ANSYS Mechanical physical preferences. Furthermore, in this analysis also, fully unstructured tetrahedral mesh is implemented throughout the surface. Curvature advance size function is employed allowing better mesh generation. The number of elements created is 206,358 and while the number of nodes created is 364,238.

2.3.3 Boundary conditions

The pressure magnitude along the propeller blade can be determined from the CFD analysis. The pressure acted on the propeller blade will cause stress distribution along the blade and deformation, resulting in performance reduction or subjective to material failure.
Structural analyses are conducted for slotted blade design for rotating speed of 3008 RPM for a range of operational velocity. This is based on the understanding that pressure generated during operation may differ based on free-stream velocity. Thus, a safe operating speed range of the propeller blade must be established to prevent damage to the material. The maximum stress generated is compared with the tensile stress at failure of the material, which is 250 MPa.

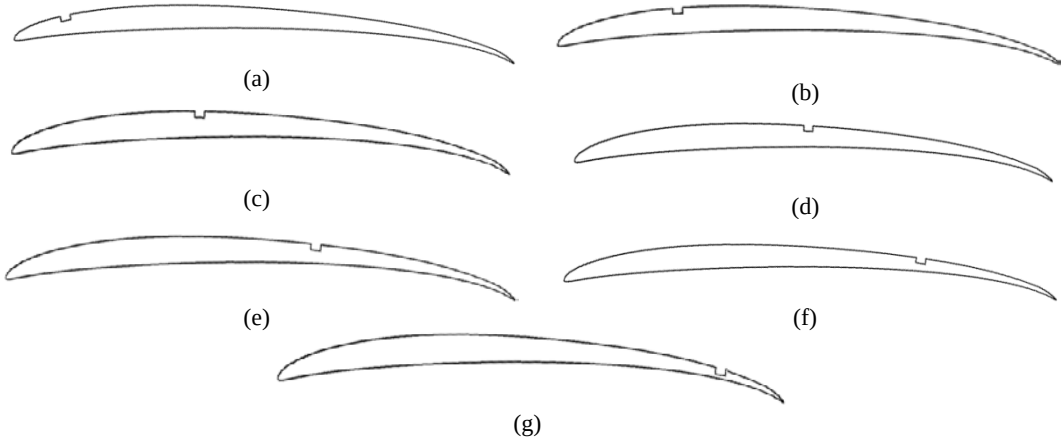

Fig. 3 - Slotted blade cross-section on the blade tip
(a) 12.5%c, (b) 25%c, (c) 37.5%c, (d) 50%c, (e) 62.5%c, (f) 75%c, (g) 87.5%c

2.4 Slotted Propeller Blade Design

Slotted propeller blade designs are tested in this study, with the intention of increasing the performance of the propeller blade through improvements of the propeller performance. This improvement can be observed either by increase in thrust, decrease in power coefficient or both. The implementation of slot in the propeller blade is expected to influence the flow around the propeller.
Fig. 3 shows the slotted blade designs analyzed in this study. The chord length of the blade remains unchanged based on baseline APC Slotted Slow Flyer and the slot dimensions are fixed for all slot positions. The slot position is altered on the basis of 12.5%c increment with respect to the chord length (c). Thus, the analysis is carried out for seven slot locations along c, which are 12.5%c, 25%c, 37.5%c, 50%c, 62.5%c, 75%c, and 87.5%c.

3. RESULTS AND DISCUSSIONS

Numerical data are compared with experimental data to validate numerical setup used throughout. The data collected from the numerical analysis are the force and the moment. Based on the data collected, the thrust coefficient, torque coefficient, power coefficient and efficiency were calculated based on Equation (1) – (7) as listed below. Equation (1) - (5) describes the thrust coefficient, torque coefficient, power coefficient, efficiency and advance ratio, respectively. Meanwhile Equation (6) and (7) shows the percentage change between the numerical method and the experimental method for the thrust and power, respectively.

$$K_T = \frac{T}{\rho n^2 D^4} \tag{1}$$

$$K_Q = \frac{P}{\rho n^2 D^5} \tag{2}$$

$$K_P = \frac{P}{\rho n^3 D^5} \tag{3}$$

$$\eta = J\frac{K_T}{K_P} \tag{4}$$

$$J = \frac{V}{nD} \tag{5}$$

$$\Delta K_T(\%) = \frac{K_{T_{CFD}} - K_{T_{EXP}}}{K_{T_{EXP}}} \times 100 \tag{6}$$

$$\Delta K_P(\%) = \frac{K_{P_{CFD}} - K_{P_{EXP}}}{K_{P_{EXP}}} \times 100 \tag{7}$$

In the equations, T(N) represents the thrust, Q(Nm) is the torque, P(W) is the power, n(rps) is represents the rotational speed, D(m) is the diameter while ρ(kgm^3) is the operational fluid density.

3.1 Numerical Method Verification and Validation

A grid independence study is conducted to determine the optimized grid for propeller performance predictions. Five grids size, referred as standard (~380,000 cells), coarse (~1,060,000 cells), mid (~2,006,000 cells), mid-fine (~3,039,000 cells) and fine (~4,093,000 cells) are generated. Fig. 4 shows the surface mesh of the propeller blade. The analyses are conducted at advance ratio of 0.628. As discussed earlier, the different grids and turbulence models were tested in this study to determine the optimal method to predict the performance of the propeller at high accuracy. Table 3 summarizes the results of the mesh independence study. Error listed indicates the discrepancy between the numerical and experimental method, calculated using Equation (6) and (7). Based on the analyses, all the meshing methods give satisfactory results with error less than 5%. The standard mesh gives optimized results for thrust, torque and efficiency. Meanwhile, other meshes show acceptable results, but with significant differences in torque and efficiency. Thus, the standard mesh is utilized throughout the entire study, as the result is sufficient to determine the performance of propeller.

In addition, Table 4 shows the results of the analyses with different turbulence models. Standard k-ω provides more accurate results compared to standard k-ε and SST k-ω. Standard k-ω manages to predict the performance for low Reynolds number applications. Thus, this turbulence model is further used throughout the analysis for this study.

Fig. 5 illustrates the results obtained during validation of the CFD results of the propeller performance. It was found that the proper correlation of numerically obtained results with experimental depends upon the advance ratio considered. It is arguable that the accuracy of numerical results is strongly influenced by the advance ratio chosen for consideration. It was observed that at low advance ratio, the thrust coefficient exhibited slight under-prediction. The

difference decreases as advance ratio increases till 0.659. For remaining higher advance ratios, a slight over-prediction was observed.

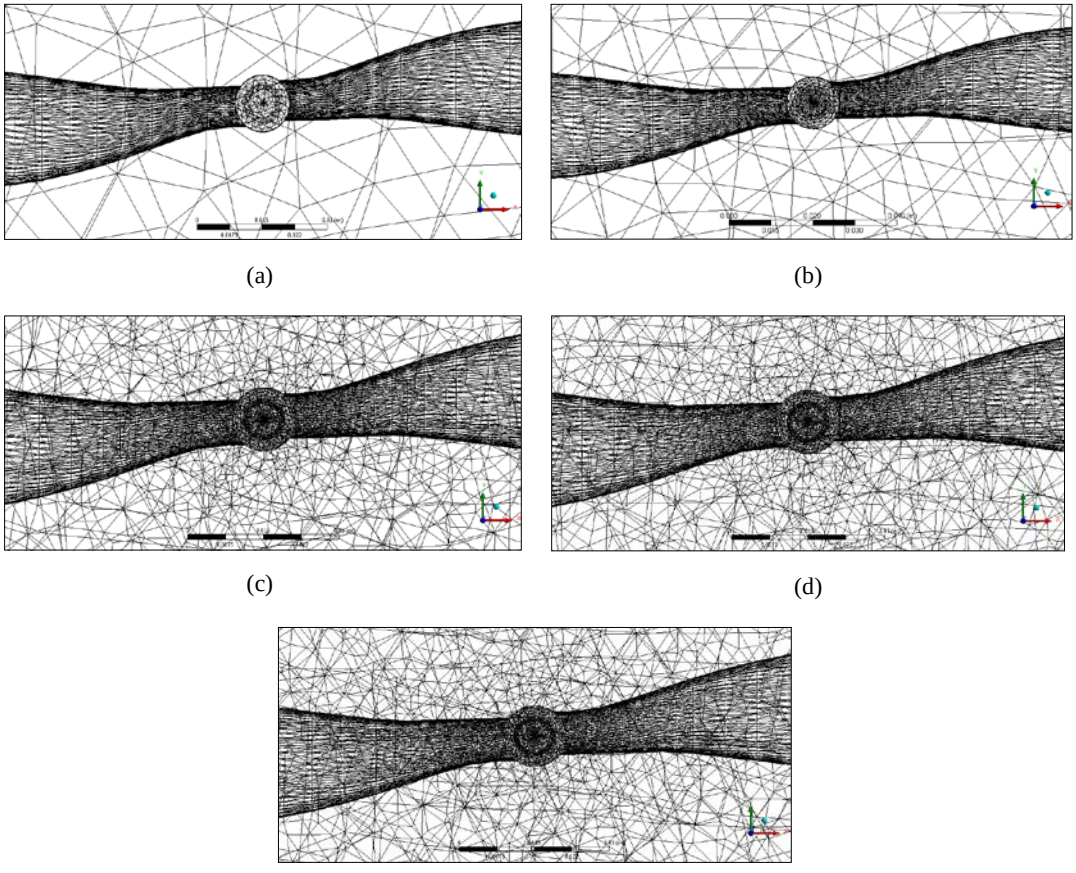

Fig. 4 - APC Slow Flyer 10’ x 7’ surface meshes. (a) Standard mesh (b) Coarse mesh (c) Mid-mesh (d) Mid-Fine mesh (e) Fine mesh

Table 3. - Computational results at different mesh resolutions with standard k-ω turbulence model for *J*=0.628

Mesh	Error (%)		
	K_T	K_Q	η
Standard	3.30	2.77	0.50
Coarse	2.38	4.15	1.89
Mid	3.33	4.01	0.77
Mid-Fine	4.42	4.02	0.38
Fine	4.35	4.26	0.38

Table 4. - Computational results with different turbulence models for *J*=0.628

Turbulence Model	Error (%)		
	K_T	K_Q	η
Standard k-ε	2.38	4.15	1.89
Standard k-ω	2.70	2.97	0.32
SST k-ω	3.42	3.88	0.53

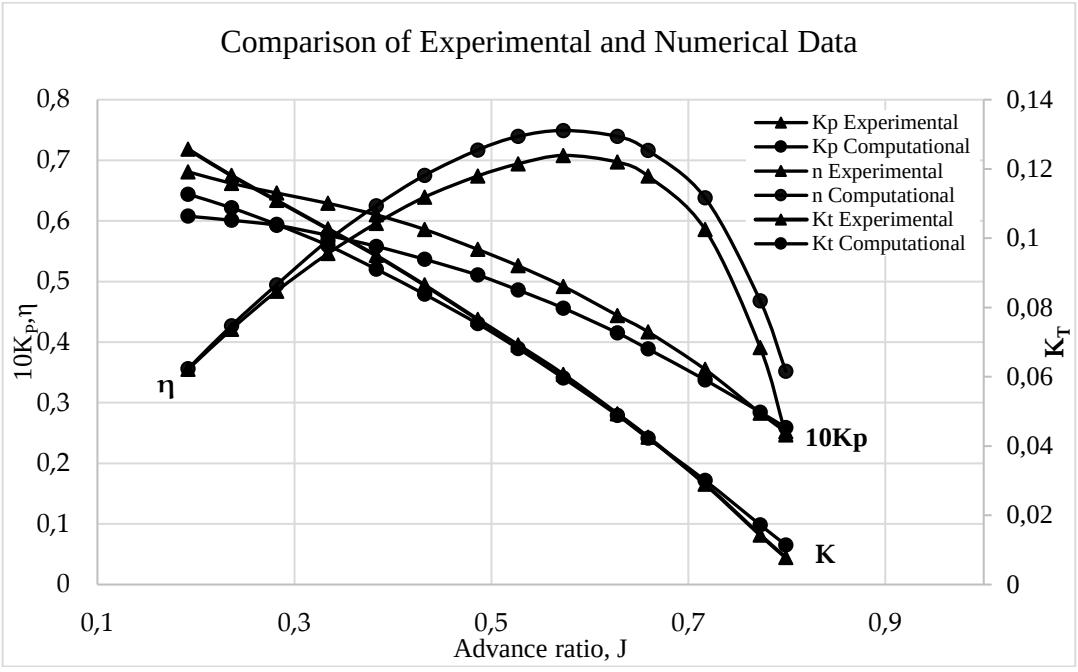

Fig. 5 - Comparisons of thrust coefficient, power coefficient, and efficiency for baseline design

With regards to power coefficient, at lower advance ratio, under-predicted results can be observed. The highest difference relative to experimental data was found for lowest advance ratio of 0.192.

In contrast, efficiency results show over-prediction for the whole range of advance ratio. It is notable that aerodynamic efficiency is the function of thrust coefficient and power coefficient. In general, the discrepancy increases as the advance ratio increases. The highest difference can be observed at advance ratio of 0.799 with a difference of 42.5% compared to experimental result.

3.2 Effect of Slot Position

The aerodynamic performance of modified propeller blade with slot is affected by the presence of slot. Fig. 6, Fig. 7 and Fig. 8 illustrate the results of the analysis for the thrust coefficient, power coefficient, and efficiency, respectively, for various slot positions compared to baseline.

Slotted design with slot at 12.5%c predicted higher thrust coefficient compared to baseline for advance ratios from 0.192 to 0.573. The increment for the aforementioned advance ratios are in the range of 0.5% to 2.44%. For the remaining advance ratios considered, the thrust coefficient was found to be decreased. The power coefficient meanwhile was found to be increased compared to baseline by about 10.38% to 33.3%.

Slotted design with slot at 25%c provided higher thrust coefficient compared to baseline. The increase in thrust coefficient can be observed for an advance ratio of up to 0.573 with difference in the range of 0.21% to 3.10%. The highest difference was observed for the advance ratio of 0.192. Beyond the aforementioned advance ratio of 0.573, the thrust coefficient decreases. The power coefficient observed was found to be higher than baseline for the entire range of advance ratios analysed. The highest difference was observed to be 44.59%.

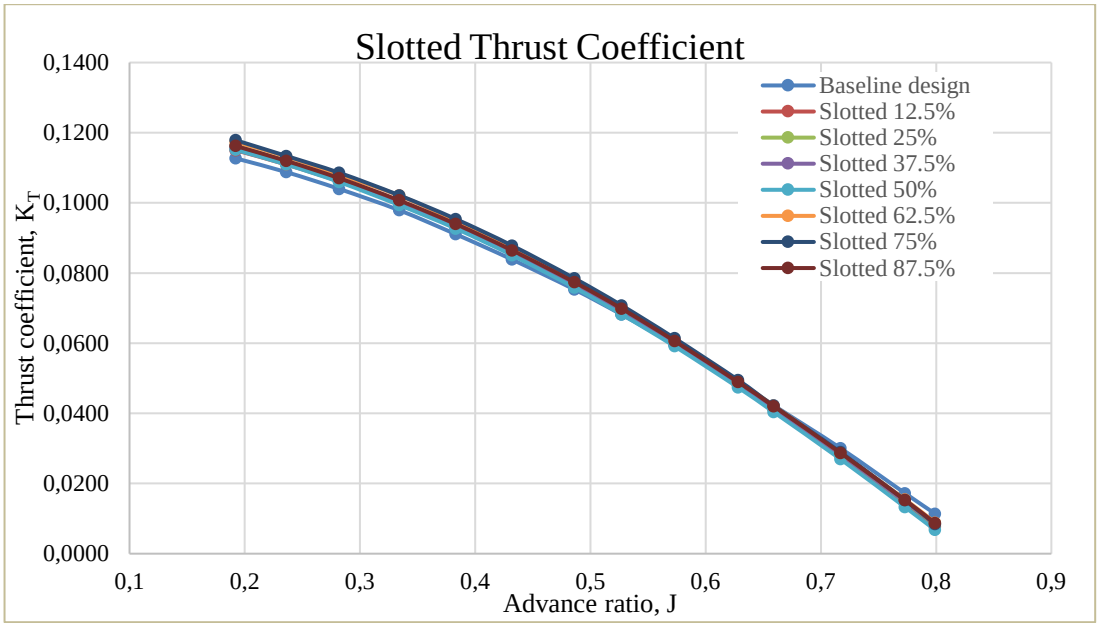

Fig. 6 - Thrust coefficient for slotted blade design for various slot positions

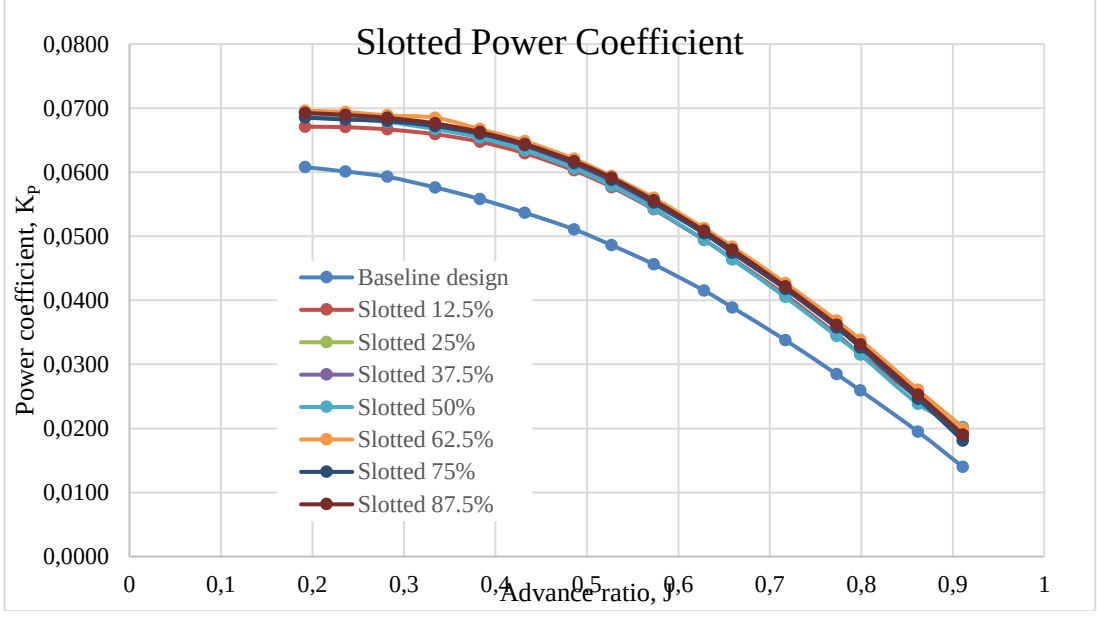

Fig. 7 - Power coefficient for slotted blade design for various slot positions

Slotted design with slot at 37.5%c showed improved thrust coefficient compared to baseline.

The highest difference in thrust coefficient between slotted and baseline design was observed at advance ratio of 0.192 with a value of 2.87%.

The power coefficient was also found to be increased compared to baseline for all advance ratios and ranges between 13.97% and 39.12%.

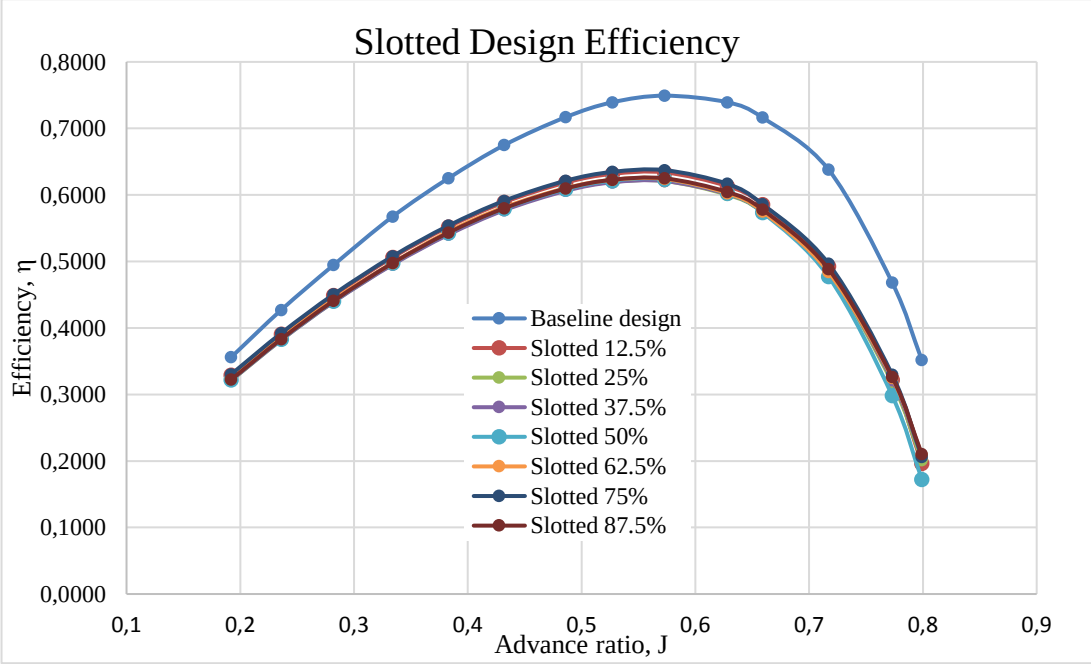

Fig. 8 - Efficiency for slotted blade design for various slot positions

Slotted design with slot at 50%c showed increase in thrust coefficient between 0.1% to 2.16% compared to baseline design for advance ratios between 0.192 and 0.573. The thrust coefficient is decreased for advance ratio from 0.573. In addition, similar to other design, an increase in thrust coefficient is also accompanied by an increase in power coefficient by 12.87% to 44.03%.

For slotted design with slot at 62.5%c, maximum thrust is generated at advance ratio of 0.334 with an increase of 4.27%. The increase in thrust coefficient can be found for advance ratios from 0.192 to 0.628. For the remaining advance ratios, the thrust coefficient was found to be decreased.

Slotted design with slot at 75%c exhibited a high increase in thrust coefficient of 4.74% compared to baseline. For advance ratio of 0.192 to 0.628, the increment was found to be in the range of 1.34% to 4.74%. A similar trend in power coefficient increase was also observed.

Slotted design with slot at 87.5%c showed increase in thrust coefficient with a maximum increase of 3.18% and minimum increase of 0.13%. The power coefficient was also found to be higher than baseline lying in the range of 13.93% to 36.14%.

From the results, it can be found that the proposed slotted blade design manages to improve the thrust for a selected range of advance ratio between 0.192 to 0.628. However, drastic increase in power coefficient was also observed. This has led to a decrease in propeller aerodynamic efficiency.

The result further shows that the propeller efficiency is dictated by the results of thrust and power. An optimal increase in thrust coefficient and a reduced power coefficient is desired. The following phenomenon can be observed. The fluid passing through the slot is incapable of being pushed back into the free-stream to prevent the flow separation. A more detailed analysis with respect to slot location is necessary for optimal design of slotted propeller with enhanced performance.

3.3 Pressure Distribution on the Propeller Blade

Each propeller design experiences different pressure distribution based on the operational condition. From ANSYS Fluent, the pressure distribution contour is generated, and the pressure will be further used for static structural analysis. Maximum and minimum pressure data is tabulated in Table 5.

Fig. 9 shows the pressure contour for the propeller blade obtained from the CFD analysis. Each of the propeller blades experience different pressure magnitude which causes stress distribution variation along the body. Based on the Fig., it can be seen clearly that the pressure at the back side of the propeller is slightly higher than the pressure at the front side of the propeller.

This condition is similar to aircraft wing, in which the pressure at the bottom of the wing is higher than that of the top side of the wing, which creates pressure difference that will generate lift for the aircraft. Meanwhile for the propeller blade, the pressure difference between the front side and back side of the propeller blade creates a force in forward direction, known as thrust. From the Fig., it can be observed that negative pressure occurs; this is due to pressure gradient that is solved using Navier Stokes equation.

Overall pressure distribution for the propeller blade is considerably uniform at the front section along the blade, compared to the back section. In addition, the leading edge experiences a higher pressure than the trailing edge, due to the flow stagnation point.

It is also shown that the free-stream speed (advance ratio) greatly influences the blade pressure distribution, where the higher the free-stream velocity, the lower the pressure difference subjected along the blade.

For free-stream velocity of 2.4384 m/s (J=0.192), the highest pressure reach 368 Pa at the back section of the blade. In addition, at free-stream velocity of 5.4864 m/s, the highest pressure observed is 574 Pa. At higher free-stream velocity, high pressure continuously occurred along the blade, especially around the trailing edge of the blade.

3.4 Stress Distribution and Deformation of Propeller Blade

The stress analysis was conducted by using ANSYS Static Structural Mechanical analysis. Structural analyses were conducted to estimate and verify the structural behaviour of the propeller blade subjected to pressure during operation. Blade stress distribution for propeller blade is shown in Fig. 10.

The results for structural analysis in term of maximum stress, maximum strain and total deformation are tabulated in Table 6. Based on the free-stream velocity, all the profile shows similar stress distribution along the blade.

Based on Fig. 10, the stress is concentrated on the hub, near to blade root area. In addition, the stress decrease with increase of radius, towards the blade tip. The stress acting on the propeller blade is highly influenced by the free-stream velocity.

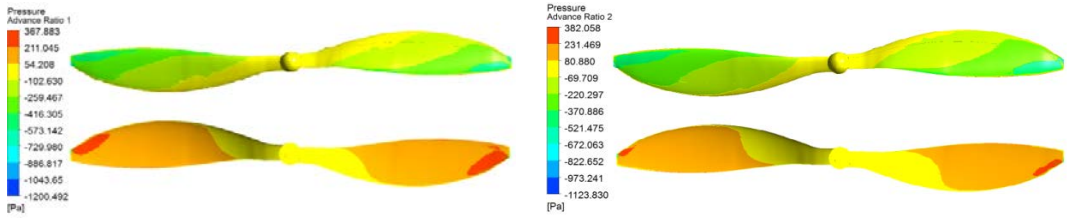

(a) (b)

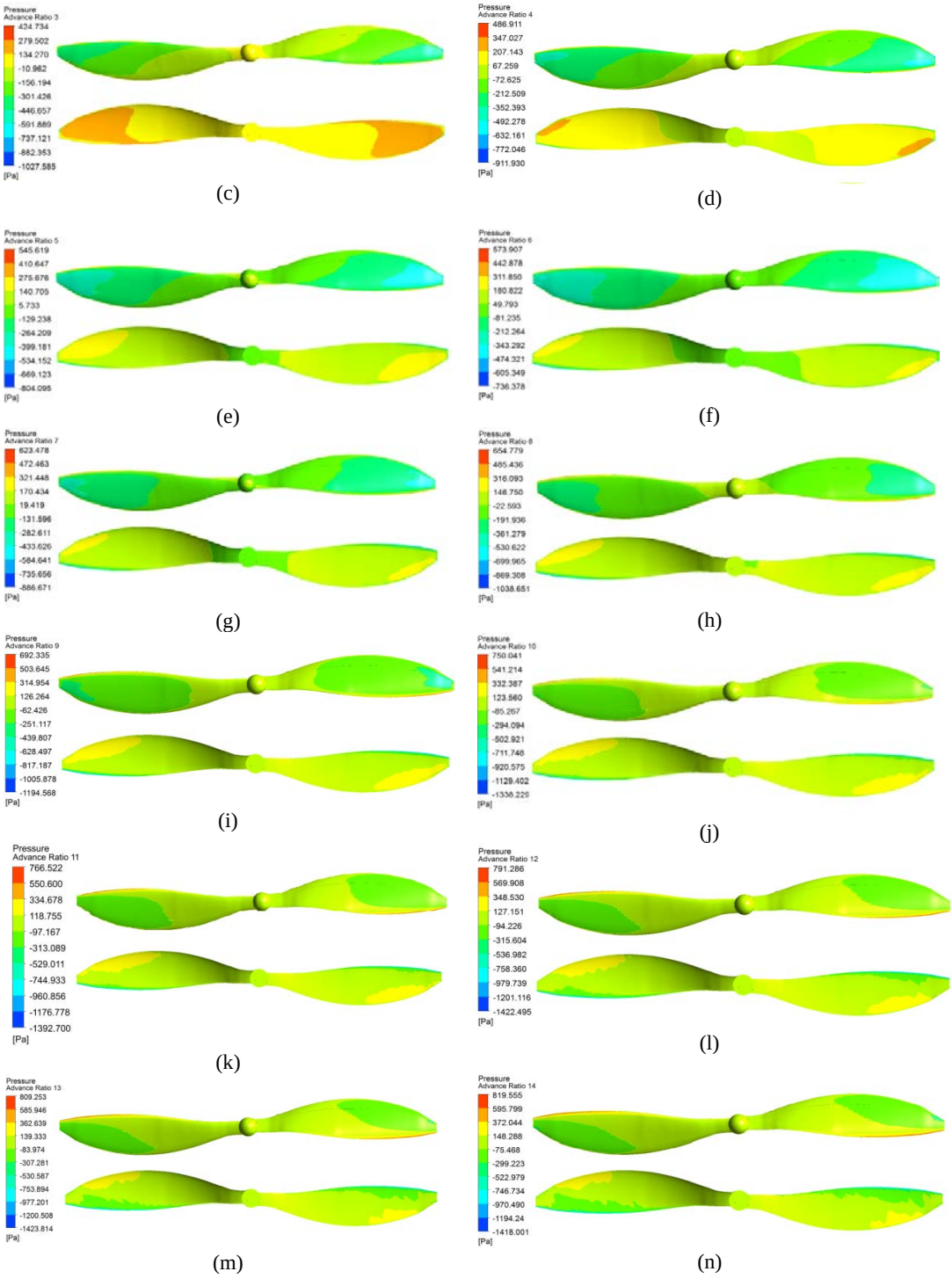

Fig. 9 - (a)-(n) Propeller blade pressure distribution at various free-stream velocity. (Top) Pressure at the front side. (Bottom) Pressure at the back side

Table 5 - Maximum and minimum pressure for slotted design

Free stream velocity (m/s)	Pressure (Pa)	
	Maximum	Minimum
2.4384	367.883	-1200.492
2.9972	382.058	-1123.83
3.5814	424.734	-1027.585
4.2418	486.911	-911.93
4.8641	545.619	-804.095
5.4864	573.907	-763.379
6.1722	623.478	-886.671
6.6929	654.779	-1038.651
7.2771	692.335	-1194.568
7.9756	750.041	-1338.229
8.3693	766.522	-1392.7
9.1059	791.286	-1422.495
9.8171	809.253	-1423.814
10.1473	819.555	-1418.001

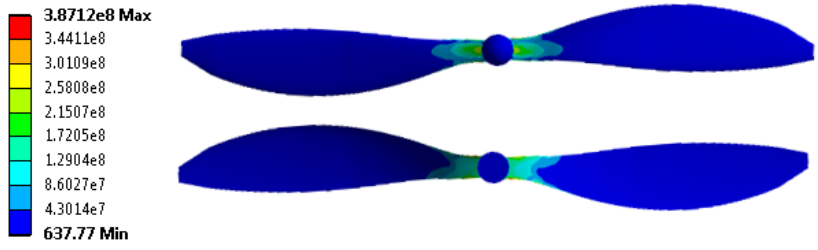

Fig. 10 - Propeller blade stress distribution
(Top) Front section (Bottom) Back section at free-stream velocity of 2.4384 m/s

For this analysis, the material selected will break under stress of 250 MPa. Thus, based on the results, the propeller will be subjected to material failure when the free-stream velocity is below 6.6929 m/s. This is because the stress due to pressure during operation exceeds the designated stress at break.

The propeller blade will be reliable for the remaining operational free-stream velocity. In addition, the material will fail when the material exceed strain at 1.58%. Based on this condition, it is suggested that the slotted propeller blade be operated only below 6.6929 m/s as it will not exceed both stress and strain at break.

Propeller blade will undergo deflection due to the load acted along the blade surface. As expected, the deformation is concentrated on the tip of the propeller blade. However, the blade material is not rigid enough to hold the shape under operational conditions, as the deformation range is so high.

Therefore, the propeller blade has higher tendency to deflect which may cause changes in the propeller performance. To overcome this issue, different material with higher rigidity may be tested.

Table 6. - Summary for static structural analysis

Free stream velocity (m/s)	Maximum Von-Mises Stress (MPa)	Maximum Von-Mises Strain (%)	Total Deformation (m)
2.4384	387.12	1.9863	0.055347
2.9972	374.15	1.9197	0.053409
3.5814	359.95	1.8469	0.051281
4.2418	340.36	1.7463	0.048358
4.8641	319.05	1.6372	0.04517
5.4864	303.67	1.5591	0.042907
6.1722	266.59	1.368	0.037437
6.6929	258.82	1.3288	0.036248
7.2771	233.9	1.2004	0.032578
7.9756	199.2	1.0227	0.02748
8.3693	181.3	0.93288	0.02453
9.1059	139.7	0.71721	0.018801
9.8171	99.656	0.51163	0.013017
10.1473	81.124	0.41649	0.010343

4. CONCLUSIONS

In this study, the performance of novel slotted propeller blade design is analysed and compared with baseline APC Slow Flyer 10'x7' propeller blade. In the analyses, the aerodynamic performance of the propeller blade is tested and the results show a desirable increase in thrust ranging from 0.1% to 4.74%. However, increase in thrust is also accompanied by increase in power coefficient, which reduces the aerodynamic efficiency of the propeller blade. This is because the propeller efficiency is directly influenced by thrust and power, which can be obtained by increase in thrust, decrease in power coefficient or both. Based on these results, further optimization is required to focus on decrease in power coefficient to ensure overall increase in propeller performance. In addition, this work also presents the pressure and stress distribution study for structural integrity of the propeller blade. Based on the analyses, the novel slotted propeller blade design managed to maintain its structural strength under during operation below 6.6929 m/s as it will not exceed both stress and strain at break. Meanwhile for deformation, higher rigidity material should be tested as the current material used in the analyses is not able to sustain the shape under operational condition. More analyses need to be performed in terms of novel propeller blade design with combination of suitable material. Therefore, high efficiency propeller blade design with high capability to sustain load under operational conditions can be achieved.

REFERENCES

[1] S. G. Kontogiannis and J. A. Ekaterinaris, Design, performance evaluation and optimization of a UAV, *Aerosp. Sci. Technol.*, vol. **29**, no. 1, pp. 339–350, 2013.

[2] R. L. Finn and D. Wright, Unmanned aircraft systems: Surveillance, ethics and privacy in civil applications, *Comput. Law Secur. Rev.*, vol. **28**, no. 2, pp. 184–194, 2012.

[3] G. Pajares, Overview and Current Status of Remote Sensing Applications Based on Unmanned Aerial Vehicles (UAVs), *Photogramm. Eng. Remote Sens.*, vol. 81, no. April, pp. 281–330, 2015.
[4] H. C. Watts, *The design of screw propellers: with special reference to their adaptation for aircraft*, First. Forgotten Books, 1920.
[5] Q. R. Wald, The aerodynamics of propellers, *Prog. Aerosp. Sci.*, vol. **42**, no. 2, pp. 85–128, 2006.
[6] X. Liu, H. Jawahar, M. Azarpeyvand, and R. Theunissen, *Aerodynamic and Aeroacoustic Performance of Serrated Airfoils*, 21st AIAA/CEAS Aeroacoustics Conf., no. June, pp. 1–16, 2015.
[7] T. P. Chong and A. Vathylakis, On the aeroacoustic and flow structures developed on a flat plate with a serrated sawtooth trailing edge, *J. Sound Vib.*, vol. **354**, pp. 65–90, 2015.
[8] M. Ibrahim, A. Alsultan, S. Shen, and R. S. Amano, Advances in Horizontal Axis Wind Turbine Blade Designs: Introduction of Slots and Tubercle, *J. Energy Resour. Technol.*, vol. **137**, no. 5, p. 51205, 2015.
[9] S. Y. Lin, Y. Y. Lin, C. J. Bai, and W. C. Wang, Performance analysis of vertical-axis-wind-turbine blade with modified trailing edge through computational fluid dynamics, *Renew. Energy*, vol. **99**, pp. 654–662, 2016.
[10] R. Belamadi, A. Djemili, A. Ilinca, and R. Mdouki, Aerodynamic performance analysis of slotted airfoils for application to wind turbine blades, *J. Wind Eng. Ind. Aerodyn.*, vol. **151**, pp. 79–99, 2016.
[11] W. Linfield, Kevin and R. G. Mudry, *Pros and Cons of CFD and Physical Flow Modeling*, 2008.
[12] J. Blazek, *Computational Fluid Dynamics: Principle and Applications*, First Edit. Baden-Daettwil, Switzerland: Elsevier, 2001.
[13] J. D. Anderson, *Computational Fluid Dynamics. The Basics with Applications*, 1st ed. New York: McGraw-Hill, 1995.
[14] J. B. Brandt and M. S. Selig, Propeller Performance Data at Low Reynolds Numbers, *49th AIAA Aerosp. Sci. Meet.*, no. January, pp. 1–18, 2011.
[15] R. W. Deters, G. K. Ananda Krishnan, and M. S. Selig, Reynolds Number Effects on the Performance of Small-Scale Propellers, in *32nd AIAA Applied Aerodynamics Conference*, 2014, no. June, pp. 1–43.
[16] S. Subhas, CFD Analysis of a Propeller Flow and Cavitation, *Int. J. Comput. Appl.*, vol. **55**, no. 16, pp. 26–33, 2012.
[17] X. Wang and K. Walters, Computational analysis of marine-propeller performance using transition-sensitive turbulence modeling, *J. Fluids Eng.*, vol. **134**, no. 7, pp. 71107-1-71107–10, 2012.
[18] Ã. E. Benini, Significance of blade element theory in performance prediction of marine propellers, *Ocean Eng.*, vol. **31**, pp. 957–974, 2004.
[19] W. Tian, B. Song, J. H. Van Zwieten, and P. Pyakurel, Computational fluid dynamics prediction of a modified savonius wind turbine with novel blade shapes, *Energies*, vol. **8**, no. 8, pp. 7915–7929, 2015.
[20] Y. R. Seetharama, K. R. Mallikarjuna, and B. S. Reddy, Stress analysis of composite propeller by using finite element Analysis, *Int. J. Eng. Sci. Technol.*, vol. **4**, no. 8, pp. 3866–3875, 2012.
[21] K. B. Yeo, W. H. Choon, and W. Y. Hau, Prediction of Propeller Blade Stress Distribution Through FEA, *J. Appl. Sci.*, vol. **14**, no. 22, pp. 3046–3054, 2014.
[22] H. N. Das, P. V. Rao, C. Suryanarayana, and S. Kapuria, Effect of Structural Deformation on Performance of Marine Propeller, *J. Marit. Res.*, vol. **X**, no. 3, pp. 47–50, 2013.
[23] S. J. Kishore, B. S. Rao, and P. K. Babu, FEM Analysis on Submarine Propeller Blade for Improved Efficiency by using Solid Works and ANSYS-Workbench, *Int. J. Emerg. Eng. Res. Technol.*, vol. **3**, no. 11, pp. 144–151, 2015.
[24] J. B. Brandt, R. W. Deters, G. K. Ananda, and M. S. Selig, *UIUC Propeller Data Site*, [Online], Available: http://m-selig.ae.illinois.edu/props/propDB.html, [Accessed: 01-Nov-2018].
[25] C. Corporation, *Celanese Technical Data*, [Online]. Available: https://www.celanese.com/, [Accessed: 23-Feb-2019].